Z. Phys. C – Particles and Fields 51, 25–35 (1991)

Zeitschrift für Physik C Particles and Fields

Search for low mass Higgs bosons produced in Z^0 decays

DELPHI Collaboration

P. Abreu[16], W. Adam[37], F. Adami[28], T. Adye[27], T. Akesson[19], G.D. Alekseev[12], P. Allen[36], S. Almehed[19], F. Alted[36], S.J. Alvsvaag[4], U. Amaldi[7], E. Anassontzis[3], P. Antilogus[15], W-D. Apel[13], B. Asman[32], P. Astier[18], J-E. Augustin[15], A. Augustinus[7], P. Baillon[7], P. Bambade[15], F. Barao[16], G. Barbiellini[34], D.Y. Bardin[12], A. Baroncelli[29], O. Barring[19], W. Bartl[37], M.J. Bates[25], M. Baubillier[18], K-H. Becks[39], C.J. Beeston[25], M. Begalli[10], P. Beilliere[6], I. Belokopytov[31], K. Belous[31], P. Beltran[9], D. Benedic[8], J.M. Benlloch[36], M. Berggren[32], D. Bertrand[2], S. Biagi[17], F. Bianchi[33], J.H. Bibby[25], M.S. Bilenky[12], P. Billoir[18], J. Bjarne[19], D. Bloch[8], P.N. Bogolubov[12], T. Bolognese[28], M. Bonapart[22], M. Bonesini[20], P.S.L. Booth[17], M. Boratav[18], P. Borgeaud[28], H. Borner[25], C. Bosio[29], O. Botner[35], B. Bonquet[15], M. Bozzo[10], S. Braibant[7], P. Branchini[29], K.D. Brand[39], R.A. Brenner[11], C. Bricman[2], R.C.A. Brown[7], N. Brummer[22], J-M. Brunet[6], L. Bugge[24], T. Buran[24], H. Burmeister[7], J.A.M.A. Buytaert[2], M. Caccia[20], M. Calvi[20], A.J. Camacho Rozas[30], J-E. Campagne[7], A. Campion[17], T. Camporesi[7], V. Canale[29], F. Cao[2], L. Carroll[17], C. Caso[10], E. Castelli[34], M.V. Castillo Gimenez[36], A. Cattai[7], F.R. Cavallo[5], L. Cerrito[29], P. Charpentier[7], P. Checchia[26], G.A. Chelkov[12], L. Chevalier[28], P. Chliapnikov[31], V. Chorowicz[18], R. Cirio[33], M.P. Clara[33], J.L. Contreras[36], R. Contri[10], G. Cosme[15], F. Couchot[15], H.B. Crawley[1], D. Crennell[27], G. Crosetti[10], N. Crosland[25], M. Crozon[6], J. Cuevas Maestro[30], S. Czellar[11], S. Dagoret[15], E. Dahl-Jensen[21], B. Dalmagne[15], M. Dam[7], G. Damgaard[21], G. Darbo[10], E. Daubie[2], P.D. Dauncey[25], M. Davenport[7], P. David[18], A. De Angelis[34], M. De Beer[28], H. De Boeck[2], W. De Boer[13], C. De Clercq[2], M.D.M. De Fez Laso[36], N. De Groot[22], C. De La Vaissiere[18], B. De Lotto[34], C. Defoix[6], D. Delikaris[7], S. Delorme[7], P. Delpierre[6], N. Demaria[33], L. Di Ciaccio[29], H. Dijkstra[7], F. Djama[8], J. Dolbeau[6], O. Doll[39], M. Donszelmann[22], K. Doroba[38], M. Dracos[7], J. Drees[39], M. Dris[23], W. Dulinski[8], R. Dzhelyadin[31], L-O. Eek[35], P.A.-M. Eerola[11], T. Ekelof[35], G. Ekspong[32], J-P. Engel[8], V. Falaleev[31], D. Fassouliotis[23], A. Fenyuk[31], M. Fernandez Alonso[30], A. Ferrer[36], T.A. Filippas[23], A. Firestone[1], H. Foeth[7], E. Fokitis[23], P. Folegati[34], F. Fontanelli[10], H. Forsbach[39], B. Franek[27], K.E. Fransson[35], P. Frenkiel[6], D.C. Fries[13], A.G. Frodesen[4], R. Fruhwirth[37], F. Fulda-Quenzer[15], K. Furnival[17], H. Furstenau[13], J. Fuster[7], J.M. Gago[16], G. Galeazzi[26], D. Gamba[33], J. Garcia[30], U. Gasparini[26], P. Gavillet[7], E.N. Gazis[23], J-P. Gerber[8], P. Giacomelli[5], K-W. Glitza[39], R. Gokieli[18], V.M. Golovatyuk[12], J.J. Gomez Y Cadenas[7], A. Goobar[32], G. Gopal[27], M. Gorski[38], V. Gracco[10], A. Grant[7], F. Grard[2], E. Graziani[29], I.A. Gritsaenko[31], M-H. Gros[15], G. Grosdidier[15], B. Grossetete[18], S. Gumenyuk[31], J. Guy[27], F. Hahn[39], M. Hahn[13], S. Haider[22], Z. Hajduk[22], A. Hakansson[19], A. Hallgren[35], K. Hamacher[39], G. Hamel De Monchenault[28], F.J. Harris[25], B.W. Heck[7], I. Herbst[39], J.J. Hernandez[36], P. Herquet[2], H. Herr[7], E. Higon[36], H.J. Hilke[7], S.D. Hodgson[25], T. Hofmokl[38], R. Holmes[1], S-O. Holmgren[32], D. Holthuizen[22], J.E. Hooper[21], M. Houlden[17], J. Hrubec[37], P.O. Hulth[32], K. Hultqvist[32], D. Husson[8], B.D. Hyams[7], P. Ioannou[3], P-S. Iversen[4], J.N. Jackson[17], P. Jalocha[14], G. Jarlskog[19], P. Jarry[28], B. Jean-Marie[15], E.K. Johansson[32], D. Johnson[17], M. Jonker[7], L. Jonsson[19], P. Juillot[8], G. Kalkanis[3], G. Kalmus[27], G. Kantardjian[7], F. Kapusta[18], P. Kapusta[14], S. Katsanevas[3], E.C. Katsoufis[23], R. Keranen[11], J. Kesteman[2], B.A. Khomenko[12], N.N. Khovanski[12], B. King[17], H. Klein[7], W. Klempt[7], A. Klovning[4], P. Kluit[2], J.H. Koehne[13], B. Koene[22], P. Kokkinias[9], M. Kopf[13], M. Koratzinos[7], K. Korcyl[14], A.V. Korytov[12], B. Korzen[7], M. Kostrikov[31], V. Kostukhin[31], C. Kourkoumelis[3], T. Kreuzberger[37], J. Krolikowski[38], U. Kruener-Marquis[39], W. Krupinski[14], W. Kucewicz[20], K. Kurvinen[11], M.I. Laakso[11], C. Lambropoulos[9], J.W. Lamsa[1], L. Lanceri[34], V. Lapchine[31], V. Lapin[31], J-P. Laugier[28], R. Lauhakangas[11], P. Laurikainen[11], G. Leder[37], F. Ledroit[6], J. Lemonne[2], G. Lenzen[39], V. Lepeltier[15], A. Letessier-Selvon[18], E. Lieb[39], E. Lillethun[4], J. Lindgren[11], I. Lippi[26], R. Llosa[36], B. Loerstad[19], M. Lokajicek[12], J.G. Loken[25], M.A. Lopez Aguera[30], A. Lopez-Fernandez[15], M. Los[22], D. Loukas[9], A. Lounis[8], J.J. Lozano[36], R. Lucock[27], P. Lutz[6], L. Lyons[25], G. Maehlum[7], N. Magnussen[39], J. Maillard[6], A. Maltezos[9], S. Maltezos[23], F. Mandl[37], J. Marco[30], M. Margoni[26], J-C. Marin[7], A. Markou[9], L. Mathis[6], F. Matorras[30], C. Matteuzzi[20], G. Matthiae[29], M. Mazzucato[26], M. Mc Cubbin[17], R. Mc Kay[1], R. Mc Nulty[17], E. Menichetti[33], C. Meroni[20], W.T. Meyer[1], W.A. Mitaroff[37], G.V. Mitselmakher[12], U. Mjoernmark[19], T. Moa[32], R. Moeller[21], K. Moenig[39], M.R. Monge[10], P. Morettini[10], H. Mueller[13], H. Muller[7], G. Myatt[25], F. Naraghi[18], U. Nau-Korzen[39], F.L. Navarria[5], P. Negri[20], B.S. Nielsen[21], B. Nijjhar[17], V. Nikolaenko[31], V. Obraztsov[31], A.G. Olshevski[12], R. Orava[11], A. Ouraou[28], R. Pain[18], H. Palka[22], T. Papadopoulou[23], L. Pape[7], A. Passeri[29], M. Pegoraro[26], V. Perevozchikov[31], M. Pernicka[37], A. Perrotta[5], M. Pimenta[16], O. Pingot[2], A. Pinsent[25], M.E. Pol[16], G. Polok[14], P. Poropat[34], P. Privitera[5], A. Pullia[20],

J. Pyyhtia[11], A.A. Rademakers[22], D. Radojicic[25], S. Ragazzi[20], W.H. Range[17], P.N. Ratoff[25], A.L. Read[24], N.G. Redaelli[20], M. Regler[37], D. Reid[17], P.B. Renton[25], L.K. Resvanis[3], F. Richard[15], M. Richardson[17], J. Ridky[12], G. Rinaudo[33], I. Roditi[7], A. Romero[33], P. Ronchese[26], V. Ronjin[31], E.I. Rosenberg[1], U. Rossi[5], E. Rosso[7], P. Roudeau[15], T. Rovelli[5], W. Ruckstuhl[22], V. Ruhlmann[28], A. Ruiz[30], H. Saarikko[11], Y. Sacquin[28], J. Salt[36], E. Sanchez[36], J. Sanchez[36], M. Sannino[10], M. Schaeffer[8], H. Schneider[13], F. Scuri[34], A.M. Segar[25], R. Sekulin[27], M. Sessa[34], G. Sette[10], R. Seufert[13], R.C. Shellard[16], P. Siegrist[28], S. Simonetti[10], F. Simonetto[26], A.N. Sissakian[12], T.B. Skaali[24], G. Skjevling[24], G. Smadja[28], G.R. Smith[27], R. Sosnowski[38], T.S. Spassoff[12], E. Spiriti[29], S. Squarcia[10], H. Staeck[39], C. Stanescu[29], G. Stavropoulos[9], F. Stichelbaut[2], A. Stocchi[20], J. Strauss[37], R. Strub[8], C.J. Stubenrauch[7], M. Szczekowski[38], M. Szeptycka[38], P. Szymanski[38], S. Tavernier[2], E. Tcherniaev[31], G. Theodosiou[9], A. Tilquin[6], J. Timmermans[22], V.G. Timofeev[12], L.G. Tkatchev[12], T. Todorov[12], D.Z. Toet[22], A.K. Topphol[4], L. Tortora[29], M.T. Trainor[25], D. Treille[7], U. Trevisan[10], W. Trischuk[7], G. Tristram[6], C. Troncon[20], A. Tsirou[7], E.N. Tsyganov[12], M. Turala[14], R. Turchetta[8], M-L. Turluer[28], T. Tuuva[11], I.A. Tyapkin[12], M. Tyndel[27], S. Tzamarias[7], F. Udo[22], S. Ueberschaer[39], V.A. Uvarov[31], G. Valenti[5], E. Vallazza[33], J.A. Valls Ferrer[36], G.W. Van Apeldoorn[22], P. Van Dam[22], W.K. Van Doninck[2], N. Van Eijndhoven[7], C. Vander Velde[2], J. Varela[16], P. Vaz[16], G. Vegni[20], J. Velasco[36], L. Ventura[26], W. Venus[27], F. Verbeure[2], L.S. Vertogradov[12], L. Vibert[18], D. Vilanova[28], N. Vishnevsky[31], E.V. Vlasov[31], A.S. Vodopyanov[12], M. Vollmer[39], G. Voulgaris[3], M. Voutilainen[11], V. Vrba[29], H. Wahlen[39], C. Walck[32], F. Waldner[34], M. Wayne[1], A. Wehr[39], P. Weilhammer[7], J. Werner[39], A.M. Wetherell[7], J.H. Wickens[2], J. Wikne[24], G.R. Wilkinson[25], W.S.C. Williams[25], M. Winter[8], D. Wormald[24], G. Wormser[15], K. Woschnagg[35], N. Yamdagni[32], P. Yepes[22], A. Zaitsev[31], A. Zalewska[14], P. Zalewski[38], E. Zevgolatakos[9], G. Zhang[39], N.I. Zimin[12], R. Zitoun[18], R. Zukanovich Funchal[6], G. Zumerle[26], J. Zuniga[36]

[1] Ames Laboratory and Department of Physics, Iowa State University, Ames, IA 50011, USA
[2] Physics Department, Univ. Instelling Antwerpen, Universiteitsplein 1, B-2610 Wilrijk, Belgium, and IIHE, ULB-VUB, Pleinlaan 2, B-1050 Brussels, Belgium, and Service de Phys. des Part. Elém., Faculté des Sciences, Université de l'Etat Mons, Av. Maistriau 19, B-7000 Mons, Belgium
[3] Physics Laboratory, University of Athens, Solonos Str. 104, GR-10680 Athens, Greece
[4] Department of Physics, University of Bergen, Allégaten 55, N-5007 Bergen, Norway
[5] Dipartimento di Fisica, Università di Bologna and INFN, Via Irnerio 46, I-40126 Bologna, Italy
[6] Collège de France, Lab. de Physique Corpusculaire, 11 pl. M. Berthelot, F-75231 Paris Cedex 05, France
[7] CERN, CH-1211 Geneva 23, Switzerland
[8] Division des Hautes Energies, CRN – Groupe DELPHI and LEPSI, B.P. 20 CRO, F-67037 Strasbourg Cedex, France
[9] Institute of Nuclear Physics, N.R.C. Demokritos, P.O. Box 60628, GR-15310 Athens, Greece
[10] Dipartimento di Fisica, Università di Genova and INFN, Via Dodecaneso 33, I-16146 Genova, Italy
[11] Dept. of High Energy Physics, University of Helsinki, Siltavuorenpenger 20 C, SF-00170 Helsinki 17, Finland
[12] Joint Institute for Nuclear Research, Dubna, Head Post Office, P.O. Box 79, SU-101000 Moscow, USSR
[13] Institut für Experimentelle Kernphysik, Universität Karlsruhe, Postfach 6980, W-7500 Karlsruhe 1, Federal Republic of Germany
[14] High Energy Physics Laboratory, Institute of Nuclear Physics, Ul. Kawiory 26a, PL-30055 Krakow 30, Poland
[15] Université de Paris-Sud, Lab. de l'Accélérateur Linéaire, Bat 200, F-91405 Orsay, France
[16] LIP, Av. Elias Garcia 14-1e, P-1000 Lisbon Codex, Portugal
[17] Department of Physics, University of Liverpool, P.O. Box 147, Liverpool L69 3BX, UK
[18] LPNHE, Universités Paris VI et VII, Tour 33 (RdC), 4 place Jussieu, F-75230 Paris Cedex 05, France
[19] Department of Physics, University of Lund, Sölvegatan 14, S-22363 Lund, Sweden
[20] Dipartimento di Fisica, Università di Milano and INFN, Via Celoria 16, I-20133 Milan, Italy
[21] Niels Bohr Institute, Blegdamsvej 17, DK-2100 Copenhagen 0, Denmark
[22] NIKHEF-H, Postbus 41882, NL-1009 DB Amsterdam, The Netherlands
[23] National Technical University, Physics Department, Zografou Campus, GR-15773 Athens, Greece
[24] Physics Department, University of Oslo, Blindern, N-1000 Oslo 3, Norway
[25] Nuclear Physics Laboratory, University of Oxford, Keble Road, Oxford OX1 3RH, UK
[26] Dipartimento di Fisica, Università di Padova and INFN, Via Marzolo 8, I-35131 Padua, Italy
[27] Rutherford Appleton Laboratory, Chilton, Didcot OX11 OQX, UK
[28] CEN-Saclay, DPhPE, F-91191 Gif-sur-Yvette Cedex, France
[29] Istituto Superiore di Sanità, Ist. Naz. di Fisica Nucl. (INFN), Viale Regina Elena 299, I-00161 Rome, Italy, and Dipartimento di Fisica, Università di Roma II and INFN, Tor Vergata, I-00173 Rome, Italy
[30] Facultad de Ciencias, Universidad de Santander, av. de los Castros, E-39005 Santander, Spain
[31] Institute for High Energy Physics, Serpukow P.O. Box 35, SU-142284 Protvino, (Moscow Region), USSR
[32] Institute of Physics, University of Stockholm, Vanadisvägen 9, S-113 46 Stockholm, Sweden
[33] Dipartimento di Fisica Sperimentale, Università di Torino and INFN, Via P. Giuria 1, I-10125 Turin, Italy
[34] Dipartimento di Fisica, Università di Trieste and INFN, Via A. Valerio 2, I-34127 Trieste, Italy, and Istituto di Fisica, Università di Udine, I-33100 Udine, Italy
[35] Department of Radiation Sciences, University of Uppsala, P.O. Box 535, S-751 21 Uppsala, Sweden
[36] Inst. de Fisica Corpuscular IFIC, Centro Mixto Univ. de Valencia-CSIC, Avda. Dr. Moliner 50, E-46100 Burjassot (Valencia), Spain
[37] Institut für Hochenergiephysik, Österreich. Akad. Wissensch., Nikolsdorfergasse 18, A-1050 Vienna, Austria
[38] Inst. Nuclear Studies and University of Warsaw, Ul. Hoza 69, PL-00681 Warsaw, Poland
[39] Fachbereich Physik, University of Wuppertal, Postfach 100127, W-5600 Wuppertal 1, Federal Republic of Germany

Received 12 February 1991

Abstract. A search for light Higgs bosons was performed using the data sample collected in 1990 by the DELPHI detector at LEP, at centre of mass energies between 88.2 and 94.2 GeV. Using the process $e^+e^- \to H^0 + Z^{0*}$, $Z^{0*} \to f\bar{f}$, it is possible to exclude the existence of the standard model Higgs particle with a mass between 0 and 210 MeV/c^2 at the 99% confidence level. Extending this analysis to the minimal supersymmetric standard model restricts the lightest neutral Higgs boson to masses above 28 GeV/c^2 irrespective of the value of the mixing angle.

1 Introduction

The standard model [1] predicts the existence of a neutral scalar Higgs particle, H^0, as well as its couplings to leptons and quarks. However the particle mass, M_{H^0}, is not constrained by the theory, and the Higgs [2] mechanism remains an unverified ingredient of the standard model and its supersymmetric extensions.

At LEP, the H^0 may be created by the process

$$e^+e^- \to H^0 + Z^{0*} \to H^0 + f\bar{f} \tag{1}$$

where the fermion pair $f\bar{f}$ can be either leptons or quarks.

This paper reports on the search for a Higgs boson with a mass below the threshold for the H^0 to decay into a muon pair, namely 210 MeV/c^2. In this mass range, the H^0 has a long lifetime. Below a few tens of MeV/c^2 it is likely to decay outside the detector while at higher mass it may decay inside the detector far from the interaction point. Two complementary analyses were made to cover the full mass range. The results can be extended to restrict the mass range for a neutral Higgs boson in the framework of the minimal supersymmetric extension of the standard model (MSSM).

Many searches for a light Higgs boson were reported by experiments done before LEP started [3]. Most of the limits obtained are affected by important uncertainties so that the only mass range reliably excluded [4] at the time was between 1.2 and 52 MeV/c^2.

Searches for light Higgs bosons were reported recently by the ALEPH [5], OPAL [6] and L3 [7] experiments at LEP.

2 The DELPHI detector

A detailed description of the DELPHI detector, of the trigger conditions and of the data reduction can be found in [8]. Here, only the specific properties relevant for this analysis are summarized.

Charged particle tracks are measured in a 1.2 T magnetic field, parallel to the beam axis. The tracking device in the barrel region consists of three cylindrical chambers: the inner detector (ID) which covers radii from 12 to 28 cm, the time projection chamber (TPC) from 30 to 122 cm and the outer detector (OD) from 197 to 208 cm. For triggering purposes, a layer of time of flight (TOF) counters is installed beyond the coil. The end caps are covered by the forward chambers A and B (FCA and FCB), at polar angles between 10° and 30° on each side.

The electromagnetic energy is measured by the high density projection chamber (HPC) in the barrel region and by the forward electro magnetic calorimeter (FEMC) in the end caps, both located after the main tracking chambers. The HPC is a high granularity lead gas calorimeter covering polar angles from 40° to 140°. A layer of scintillators is installed after the first 5 radiation lengths and used for fast triggering. The FEMC is composed of lead glass blocks covering polar angles from 10° to 36°.

Unless otherwise stated, two trigger components were used in the analysis. The first one requires a back-to-back coincidence of OD quadrants together with any signal from the ID. The second one is made by coincidences of the HPC and TOF scintillation counters. Details about these components can be found in [9].

3 Search for a Higgs boson decaying outside the detector

The average decay length of a light Higgs boson is given in meters by the formula $6.3 \cdot (40/M_{H^0})^2$, where M_{H^0} is expressed in MeV/c^2. If the H^0 mass is below a few tens of MeV/c^2, the particle has a very long lifetime and is likely to decay outside the detector. The small effect of a missing low mass H^0 can only be detected in the decay of the Z^{0*} to a muon or electron pair. Therefore, we restrict the search in this analysis to light Higgs particles produced in association with a muon or electron pair and which decay outside the components of the detector that are sensitive to electrons or photons. Furthermore, we have to separate possible candidates from the radiative events $l^+l^-\gamma$, using the different angular distributions and the possible detection of the additional photon.

3.1 Selection of Higgs candidates

The main source of background comes from radiative Z^0 leptonic decays in which the photon escapes detection:

$$e^+e^- \to Z^0 \to l^+l^- + (\gamma) \tag{2}$$

or from τ pair production with only two charged particles in the final state:

$$e^+e^- \to Z^0 \to \tau^+\tau^- \to \text{two charged particles.} \tag{3}$$

Monte Carlo samples of events from reaction (1) and from background processes (2) and (3) were used to define the selection criteria and to determine their efficiencies, as well as to calculate the trigger efficiency and acceptance for process (1). We use the event generator described in [10] for the reaction (1) and the event generators KORALZ [11] and DYMU3 [12] for the background processes. The simulated raw data were passed

through the same reconstruction and analysis programs as the real data.

In order to reduce the background coming from the radiative Z^0 leptonic decay, including events where the photon goes along the beam pipe, we have optimized a cut on the leptonic pair acoplanarity (defined as the complement of the angle formed by the two charged leptons in the plane perpendicular to the beam). This cut also reduces the τ background events.

An event is considered as a Higgs candidate if the following requirements are fulfilled:

1. The event has only two charged particles, both coming from a region surrounding the collision point within 10 cm along the beam direction and within 2 cm in the transverse plane.
2. The particles have a momentum larger than 20 GeV/c (in order to reduce contamination from the τ background) and their trajectories are required to be at more than 30° to the beam direction.
3. The acoplanarity of the final leptons is greater than 5°. Figure 1 shows the acoplanarity distribution for real (crosses) and simulated (full line) $\mu^+\mu^-$, e^+e^- and $\tau^+\tau^-$ events passing selections 1 and 2, with quite satisfactory agreement between data and Monte Carlo.
4. The electromagnetic energy deposits not associated to charged tracks do not exceed 2 GeV. This cut eliminates the leptonic events with a hard radiated photon, except those for which the photon remains unseen.
5. There is no evidence for a shower in the direction of the missing momentum. This requirement rejects events of type (2) in which the photon is not well detected due to gaps between the sensitive regions of the electromagnetic calorimeters. For such events, although the photon energy is not completely reconstructed in the HPC or FEMC modules there is usually evidence of its presence.

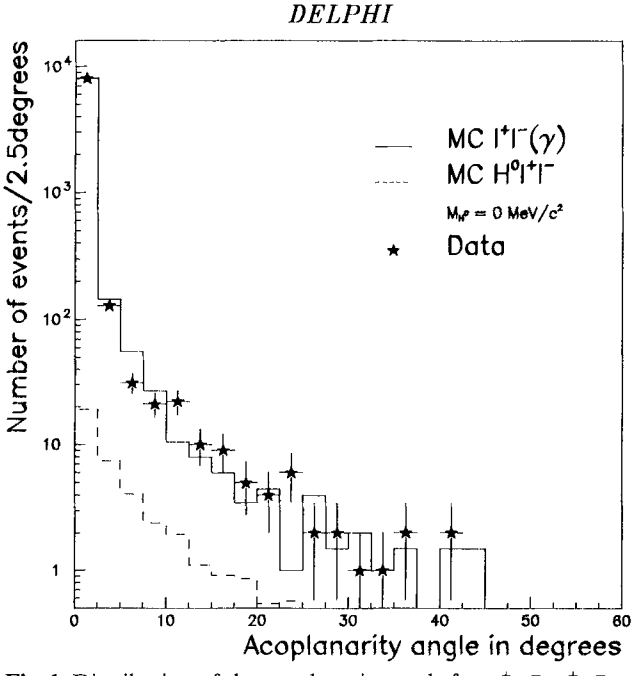

Fig. 1. Distribution of the acoplanarity angle for $\mu^+\mu^-$, e^+e^- and $\tau^+\tau^-$ events after selections on momentum and polar angle only. The data are shown by crosses and the Monte-Carlo by a full line. The dashed line shows the same distribution for a zero mass Higgs boson

Table 1. Overall detection efficiencies for $H^0 l^+ l^-$ (l=e, μ)

m_{H^0} (MeV/c²)	efficiency (%) $l=\mu$	efficiency (%) l=e
0	23.6 ±0.8 ±1.3	21.8 ±0.7 ±1.2
10	23.3 ±0.8 ±1.3	21.6 ±0.7 ±1.2
20	19.9 ±0.7 ±1.1	18.4 ±0.6 ±0.9
30	16.7 ±0.6 ±0.9	15.5 ±0.5 ±0.8
40	12.4 ±0.4 ±0.7	11.5 ±0.4 ±0.6
50	10.0 ±0.3 ±0.5	9.4 ±0.3 ±0.5
70	4.8 ±0.2 ±0.3	4.5 ±0.1 ±0.2
100	1.24±0.04±0.06	1.15±0.04±0.06

After applying selections 1 to 4 to samples of simulated events of types (1), (2) and (3), the fraction of background dilepton pairs which survive the selection criteria, is (0.12±0.02)%, while the Higgs selection efficiencies for a zero mass Higgs, are (25.5±0.7)% for the muon channel and (22.6±0.7)% for the electron channel. The background contamination is further reduced to (0.05±0.01)% by the last selection (5) without affecting the selection efficiencies for a zero mass Higgs.

The trigger efficiency corrected for the acceptance for this analysis was determined from our simulation. It was found to be (92.5±1.7)% for the muon channel and (96.5±1.3)% for the electron channel, independent of the Higgs mass. The quoted uncertainties are purely statistical. A conservative 5% systematic uncertainty on the selection efficiency was estimated by checking the sensitivity of the results to cuts 3 and 4, while a 2% systematic uncertainty on the trigger efficiency was estimated from the trigger simulation program.

Table 1 shows the overall detection efficiency and the related statistical and systematic uncertainties as a function of M_{H^0} for both channels.

The data sample used for the analysis is equivalent to 53139 hadronic $Z^0 s$ and corresponds to an integrated luminosity of 2515 nb^{-1}. Only 4 events survive the first four selections, consistent with the expected background contamination of 5.9±1.2±0.2 events.

The 4 candidates show evidence for a converted photon in the direction of the missing momentum and are therefore rejected by the final selection 5.

Table 2. Number of expected events for $H^0 l^+ l^-$ (l=e, μ)

m_{H^0} (MeV/c²)	Number of expected events
0	12.03±0.29±0.52
10	11.89±0.29±0.51
20	10.15±0.24±0.44
30	8.54±0.21±0.37
40	6.33±0.15±0.28
50	5.09±0.12±0.22
70	2.46±0.06±0.11
100	0.63±0.02±0.03

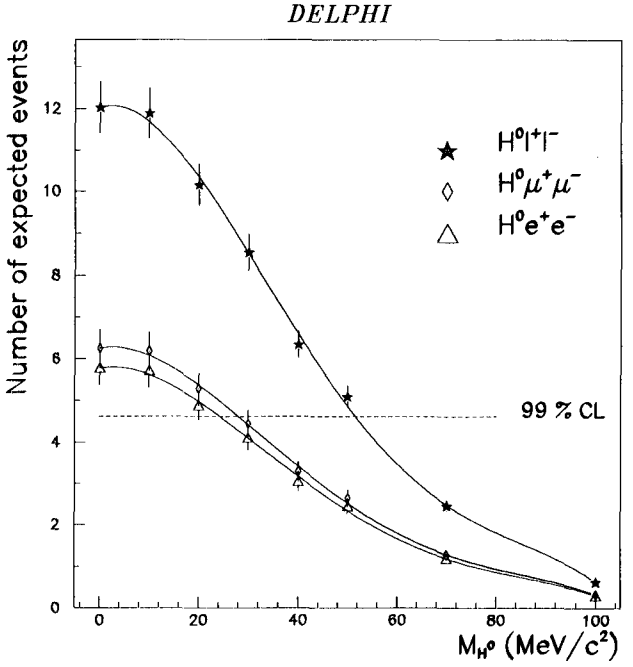

Fig. 2. Numbers of selected H^0 events predicted using the standard model. The error bars represent the systematic and statistical uncertainties added in quadrature. The 99% confidence level for the possible signal is given by the dashed line

3.2 Results

The expected number of $H^0 l^+ l^- (l = e, \mu)$ events in the standard model is given in Table 2 as a function of M_{H^0}. Figure 2 shows the expected signal. Given the fact that no candidate survives the selection procedure, a light Higgs boson is excluded up to a mass of 52 MeV/c^2 at the 99% confidence level.

4 Search for a Higgs boson decaying inside the detector

If the mass of the Higgs boson is larger than a few tens of MeV/c^2, the average decay length of the particle is inside the detector. As an example, for a mass of 100 MeV/c^2, the rest lifetime is $\tau^0 = 0.5\,10^{-10}$ s, which corresponds to an average decay length $\beta\gamma c\tau$ of the order of 1 meter. Below the two muon threshold, the particle decays predominantly into an e^+e^- pair, the branching ratio of the other possible decay, $H \to \gamma\gamma$ being of the order of 10^{-3} in the standard model with three generations [13]. Therefore, a Higgs boson decaying inside the detector will lead to a pair of tracks coming from the same point (V^0) and recoiling against the decay products of a virtual Z^0 produced practically at rest. The H^0 is emitted almost isotropically so that the V^0 is most often isolated in the event.

The main sources of background are Z^0 decays in which a radiative photon is converted in the detector material, hadronic Z^0 decays producing a longlived neutral hadron or a neutral pion decaying into two photons and $\gamma\gamma$ processes which produce a prompt pair of collimated tracks. The latter type of background is also expected from rare four-fermion processes in which a virtual photon is radiated from one of the decay products of the Z^0 [14].

Three analyses were made to take into account, not only the leptonic channels, but also the neutrino and hadronic Z^0* decays. In all cases, we select Z^0-like events containing a V^0 and apply restrictions on the V^0 decay position, momentum, mass and isolation in order to suppress the backgrounds. The same V^0 reconstruction algorithm is used throughout the analysis but the restrictions on the V^0 features depend on the channel.

4.1 V^0 reconstruction

The V^0 reconstruction method uses the tracking devices of the central region of DELPHI. The detectors concerned are the time projection chamber (TPC), the inner detector (ID) and the outer detector (OD). A search is made for pairs of tracks of opposite charge, which either cross each other or are tangential in the transverse plane with respect to the beam axis. If the tracks cross each other, the decay vertex of the pair is taken as the crossing point which has the smallest difference in the z coordinates (that is, coordinates along the beam axis). Two tracks are considered as tangential if their minimal distance of approach in the transverse plane is less than 5 mm. In this case, the vertex is defined as the middle of the minimal segment between the two tracks in the transverse plane; its z coordinate is the average of the z coordinates of the segment ends. To keep a pair of tracks as a V^0 candidate, the z difference between the tracks at the decay vertex must be less than 5 mm and the vertex itself must be at least 2 cm away from the beam axis. Moreover, the V^0 momentum, defined as the sum of the track momenta at the decay vertex, must point back to the primary vertex within an angular tolerance of 5°.

The crucial point for the Higgs boson search is the V^0 reconstruction efficiency. When the angle between the two V^0 tracks is small (less than about 20 mrad), which is the case for a very low mass Higgs particle, the two tracks cannot be separated in the neighbourhood of the decay point. Coordinates are poorly measured in this region, which affects the pattern recognition. The V^0 reconstruction efficiency is then strongly dependent on the radial position of the decay vertex, on the V^0 polar angle, and on the mass of the decaying particle. To study this efficiency, we used simulated $H\nu\bar{\nu}$ samples for several Higgs masses and we divided the detector into five fiducial regions where the efficiency is expected to remain the same. The study showed that one cannot expect to reconstruct a V^0 decaying more than 80 cm away from the beam axis because the TPC external radius is only 120 cm. All the criteria used to define a V^0 were tuned both on simulated $H\nu\bar{\nu}$ and $q\bar{q}$ data and on the sample of K^0s, Λs and converted photons observed in real data, to ensure that the actual efficiency of detection is well represented by the Monte Carlo. As an example, Fig. 3 shows the distribution of the conversion radius of photons detected in hadronic Z^0 events.

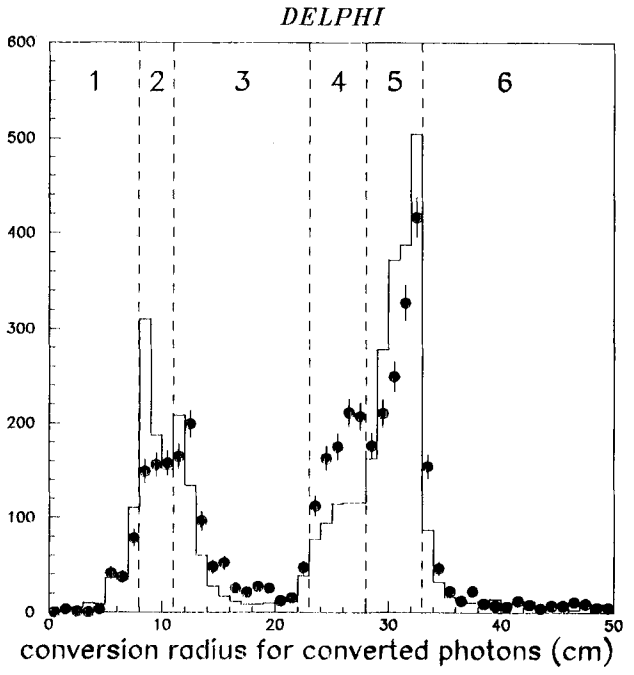

Fig. 3. Conversion radius for γs produced in hadronic Z^0 decays, as observed in real data (points) and simulated data (histogram). Six regions can be recognized: vacuum chamber (1), beam pipe and vertex detector (2), Inner Detector jet chamber (3) and trigger chamber (4), Time Projection Chamber inner vessel (5) and gas volume (6). The initial samples of real and simulated hadronic events are normalized to each other

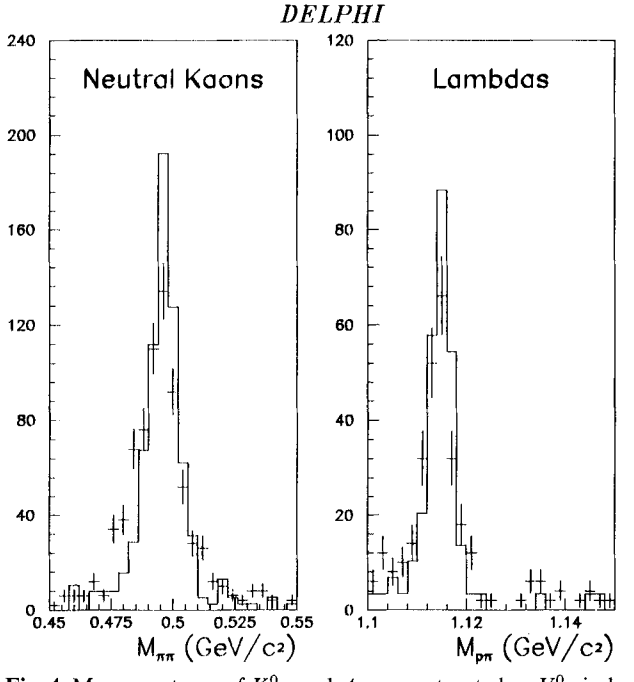

Fig. 4. Mass spectrum of $K^0 s$ and Λs reconstructed as $V^0 s$ in hadronic Z^0 decays. The $(\pi\pi)$ invariant mass of a V^0 is calculated assuming that both particles of the pair are pions while the $(p\pi)$ invariant mass is calculated assuming that the more energetic particle of the pair is a proton. The distributions for the real data (crosses) and for the simulated ones (histogram) are normalized to each other, to check the resolution of the V^0 reconstruction algorithm

The agreement between data and Monte Carlo is satisfactory for the purposes of the analysis, although the position of the radiating material is not perfectly simulated. Figure 4 gives the mass spectrum for $K^0 s$ and Λs showing that neutral kaons are reconstructed with a FWHM equal to 15 MeV/c^2. The agreement between data and Monte Carlo is adequate for our study, even though the observed distributions are shifted by 2 MeV/c^2. Finally, the V^0 reconstruction efficiency in the fiducial volume ($R<80$ cm, $45°<\theta<135°$) is estimated to be $(76.0\pm4.0)\%$ for a Higgs mass of 50 MeV/c^2.

4.2 Higgs boson produced with charged leptons

Candidates for the channels $H^0 e^+ e^- \rightarrow$ and $H^0 \mu^+ \mu^-$ must obey the following selection criteria:

1. Four tracks reconstructed in the TPC.
2. Two tracks of opposite charges and momenta larger than 3 GeV/c, each of them lying in the central region (i.e. with polar angles between 40° and 140°) and coming from the interaction point. The total visible energy of the two tracks must be larger than 10 GeV and their acolinearity angle smaller than 60°.
3. A reconstructed V^0 in the central region, with at least 500 MeV/c of transverse momentum with respect to the beam axis and with an isolation angle from the closest track larger than 40°.
4. The reconstructed V^0 mass assuming that both tracks are electrons is above 10 MeV/c^2. This cut is introduced to reduce the main background coming from dilepton events with a hard γ converted in the inner vessel of the TPC (4% of a radiation length). The reconstructed

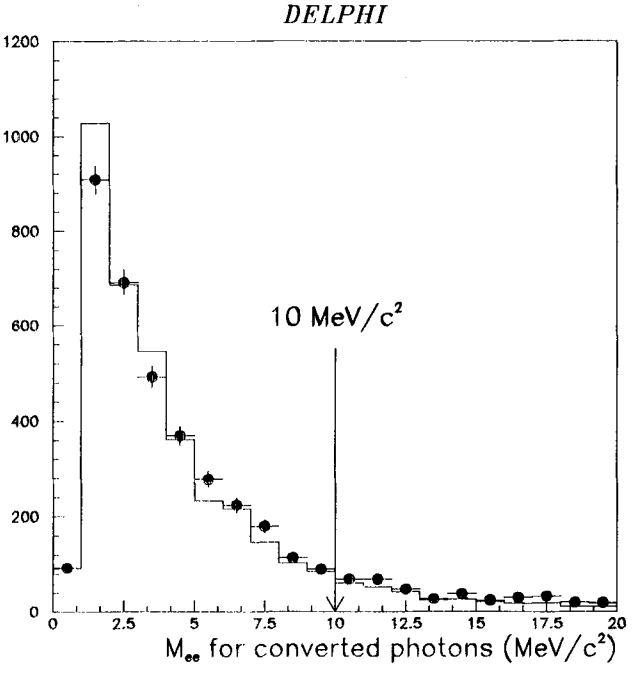

Fig. 5. Mass spectrum for converted γ's observed in the same data sample of hadronic Z^0 decays as in Fig. 3. The points stand for real data and the histogram for simulated ones. The initial samples of real and simulated hadronic events are normalized to each other

Table 3. Overall detection efficiency and expected signal for $H^0 e^+ e^-$

m_{H^0} (MeV/c^2)	Efficiency (%)	Expected signal
25	$2.1 \pm 0.6 \pm 0.2$	$0.6 \pm 0.2 \pm 0.1$
50	$10.2 \pm 1.3 \pm 1.0$	$3.1 \pm 0.4 \pm 0.3$
100	$13.9 \pm 1.5 \pm 1.4$	$4.3 \pm 0.5 \pm 0.5$
150	$16.5 \pm 1.6 \pm 1.7$	$5.1 \pm 0.5 \pm 0.6$
200	$13.7 \pm 1.5 \pm 1.4$	$4.2 \pm 0.5 \pm 0.5$

Table 4. Overall detection efficiency and expected signal for $H^0 \mu^+ \mu^-$

m_{H^0} (MeV/c^2)	Efficiency (%)	Expected signal
25	$3.1 \pm 0.5 \pm 0.3$	$1.0 \pm 0.2 \pm 0.1$
50	$7.8 \pm 0.9 \pm 0.8$	$2.4 \pm 0.3 \pm 0.3$
100	$14.7 \pm 1.2 \pm 1.5$	$4.5 \pm 0.4 \pm 0.5$
150	$18.2 \pm 1.3 \pm 1.9$	$5.6 \pm 0.4 \pm 0.6$
200	$17.6 \pm 1.3 \pm 1.8$	$5.4 \pm 0.4 \pm 0.6$

mass spectrum for such pairs typically lies below 5 MeV/c^2, as can be seen in Fig. 5.

The restriction to the central region arises from the need for a well controlled trigger efficiency: in this region, the trigger efficiencies [15] are $(97 \pm 2)\%$ in the $\mu^+ \mu^-$ channel and 100% with a negligible uncertainty in the $e^+ e^-$ channel. The trigger acceptance and the efficiency of the selection criteria were monitored on simulated events. The overall detection efficiencies including all effects are given in Tables 3 and 4, together with the related statistical and systematic uncertainties.

The $H^0 \tau^+ \tau^-$ final states can be selected in the same way if both τ decays yield only one charged particle, since the cut on the acolinearity angle is loose enough (60°). To extend the analysis to topologies where the two τs decay respectively into 1 and 3 charged particles, the same selections were applied with the following modification for cuts 1 and 2:

1. Six tracks reconstructed in the TPC.
2. One isolated track of momentum above 1 GeV/c and three tracks of momenta above 100 MeV/c contained in a 20° half-angle cone around their resultant momentum axis. This axis and the direction of the isolated particle must lie in the central region and the acolinearity angle between them must be smaller than 60°.

The trigger efficiency is the same as in the $\mu^+ \mu^-$ channel. The overall detection efficiencies are shown in Table 5.

Table 5. Overall detection efficiency and expected signal for $H^0 \tau^+ \tau^-$

m_{H^0} (MeV/c^2)	Efficiency (%)	Expected signal
25	$1.9 \pm 0.3 \pm 0.2$	$0.6 \pm 0.1 \pm 0.1$
50	$4.9 \pm 0.6 \pm 0.5$	$1.5 \pm 0.2 \pm 0.2$
100	$9.1 \pm 0.8 \pm 0.9$	$2.8 \pm 0.2 \pm 0.3$
150	$11.3 \pm 0.8 \pm 1.1$	$3.5 \pm 0.3 \pm 0.4$
200	$11.9 \pm 0.8 \pm 1.1$	$3.4 \pm 0.2 \pm 0.4$

The main factors explaining the low efficiencies in the charged leptonic channels are the restriction of all tracks to the barrel region, the H^0 decay probability in the fiducial region, the V^0 reconstruction efficiency and the requirement on the V^0 isolation. The data sample used for the analysis corresponds to an integrated luminosity of 2496 nb^{-1}. No candidate was found.

4.3 Higgs boson produced with neutrinos

The branching ratio into the $H \nu \bar{\nu}$ final state is six times larger than into each of the charged leptonic channels, and the backgrounds are easily suppressed.

We first select events with one V^0 and no other charged particles, which are mostly forward radiative Bhabhas. The following additional selections are then applied:

1. V^0 polar angle in the central region, that is between 40° and 140°. This is a powerful selection against radiative Bhabhas.
2. Momentum of each particle of the pair above 200 MeV/c and V^0 transverse momentum with respect to the beam axis above 1 GeV/c, in order to remove events from two photon processes.
3. No energy deposition in the luminosity monitor nor in the forward electromagnetic calorimeters to remove Bhabhas and events from two photon processes.
4. No back-to-back deposits of more than 20 GeV in the HPC to remove radiative pairs whose tracks are lost in the gaps between adjacent sectors of the TPC.

The main difficulty for this channel is to determine the trigger efficiency. It was evaluated conservatively selecting the two relevant triggers with a well controlled efficiency. The first one requires a coincidence between at least one trigger layer of the inner detector and at least two different sectors of the outer detector. Its efficiency is $(94 \pm 2)\%$. The second one is a single track trigger requiring at least one track fully contained in one sector of the TPC. Its efficiency is $(95 \pm 2)\%$. These trigger components are only sensitive to $V^0 s$ decaying respectively before the inner detector and before the very beginning of the TPC. For this reason, the overall detection efficiency is expected to fall faster at low masses than for the charged leptonic channels.

The results are given in Table 6. The main contribution to the inefficiency in this channel is the geometrical acceptance of the trigger components. As the two trig-

Table 6. Overall detection efficiencies and total expected signal for $H^0 \nu \bar{\nu}$

m_{H^0} (MeV/c^2)	Efficiency 1 (%)	Efficiency 2 (%)	Expected signal
25	$0.6 \pm 0.2 \pm 0.1$	$1.6 \pm 0.4 \pm 0.2$	$0.7 \pm 0.1 \pm 0.1$
50	$0.3 \pm 0.2 \pm 0.1$	$3.5 \pm 0.6 \pm 0.4$	$1.1 \pm 0.2 \pm 0.1$
100	$3.5 \pm 0.6 \pm 0.4$	$14.0 \pm 1.1 \pm 1.4$	$5.5 \pm 0.5 \pm 0.5$
150	$4.8 \pm 0.7 \pm 0.5$	$19.6 \pm 1.3 \pm 2.0$	$7.7 \pm 0.6 \pm 0.7$
200	$7.5 \pm 0.9 \pm 0.8$	$23.3 \pm 1.4 \pm 2.4$	$9.9 \pm 0.6 \pm 0.9$

gers were not introduced at the same time in the data taking, two sets of selection efficiences were computed. The first one includes only the trigger component based on the inner and outer detectors, while the second set takes both components into account. The related data samples correspond to integrated luminosities of respectively 722 nb^{-1} and 387 nb^{-1}. Only one event fulfills the first three selection criteria. This event has two back-to-back high energy deposits (43 GeV and 39 GeV) in the barrel electromagnetic calorimeter, as well as hits in the inner and outer detectors in the direction of the energy clusters. It is thus identified as a radiative e^+e^- event where both electrons remain undetected and is rejected by condition 4.

4.4 *Higgs boson produced with hadrons*

The $H^0q\bar{q}(g)$ channel may be a good source of H^0 because it includes 70% of all $H^0f\bar{f}$ channels. One must search for hadronic Z^0 events with at least one isolated V^0. This channel suffers from a very large background, arising mostly from the photons produced in π^0 decays ($\pi^0 \to \gamma\gamma$) as well as from strange neutral hadrons at higher masses (K's and Λ's). Also, an increase of the contamination from fake V^0s is expected due to the high event multiplicities. Therefore, the V^0 definition was modified: pairs of tangential tracks are no longer accepted as V^0 candidates and the tolerance applied to the angle between the V^0 momentum and its line of flight is decreased from 5° to 2°. The event selection criteria are then the following:

1. At least six charged tracks with momenta above 100 MeV/c and with polar angles between 25° and 155°. The tracks extrapolate back to within 5 cm from the beam axis in r and within 10 cm from the crossing point in z. The total charged energy in each of the two forward-backward hemispheres exceeds 3 GeV, while the total charged energy of the event exceeds 15 GeV. The polar angle of the sphericity axis lies between 30° and 150°.
2. One reconstructed V^0 in the central region, with at least 1 GeV/c of transverse momentum with respect to the beam axis, the momentum of each particle of the pair being larger than 200 MeV/c.
3. No charged particle with a momentum above 100 MeV/c within a 30° half-angle cone around the V^0 direction and no charged particle with a momentum above 1 GeV/c within a 40° half-angle cone around the same direction.
4. Radius of the V^0 decay point greater than 5 cm to remove fake V^0s and outside the following ranges (Fig. 3): $8\,\text{cm} < r < 12\,\text{cm}$ and $22\,\text{cm} < r < 34\,\text{cm}$ to remove photon conversions. To reinforce the suppression of converted photons, the reconstructed V^0 mass assuming that both tracks are electrons is required to be above 10 MeV/c^2 (Fig. 5).
5. V^0s whose $p\pi$ mass lies between 1100 MeV/c^2 and 1130 MeV/c^2 or whose e^+e^- mass is larger than 250 MeV/c^2 are excluded, in order to remove long-lived neutral hadrons. Using the e^+e^- mass instead of the $\pi\pi$ mass in the last condition removes all K^0s without losing any Higgs boson in the mass range below 210 MeV/c^2.

Table 7. Overall detection efficiency and expected signal for $H^0q\bar{q}$

m_{H^0} (MeV/c^2)	Efficiency (%)	Expected signal
25	$0.4 \pm 0.2 \pm 0.1$	$2.3 \pm 1.3 \pm 0.2$
50	$1.7 \pm 0.4 \pm 0.2$	$9.0 \pm 2.0 \pm 1.0$
100	$2.8 \pm 0.5 \pm 0.3$	$15.0 \pm 2.8 \pm 1.6$
150	$2.7 \pm 0.6 \pm 0.3$	$14.9 \pm 3.5 \pm 1.6$
200	$2.6 \pm 0.6 \pm 0.3$	$14.2 \pm 3.4 \pm 1.6$

The trigger efficiency for this channel is $(100 \pm 2)\%$. The overall detection efficiencies are of the order of a few percent, which is mainly due to more stringent V^0 selection criteria than in the previous sections (see Table 7). The analysis was performed on a data sample corresponding to an integrated luminosity of 2109 nb^{-1}. Four events satisfied the selection criteria. For all of them, the reconstructed e^+e^- mass of the V^0 candidate is below 50 MeV/c^2. For two events, the V^0 is probably a γ converted in the beam pipe, which is not rejected by cut 4 because of the uncertainty in the measurement of the V^0 decay radius. The V^0 of the third event is accompanied by a soft photon close to the direction of its momentum, and its vertex is very near the inner wall of the TPC, so it may be interpreted as a converted γ coming from a π^0 decay. Finally, the V^0 of the last event can be interpreted as a γ converted in the central high voltage plate of the TPC. A study of simulated hadronic events shows that the expected background is 4.0 ± 2.0 events, which is consistent with what is observed, including the fact that the e^+e^- mass of the reconstructed V^0 in the selected background events is smaller than 50 MeV/c^2.

4.5 *Results*

Figure 6 shows the expected Higgs signal in the leptonic channels only, as a function of the Higgs boson mass. No candidate being observed, the following Higgs mass range can be excluded at the 99% confidence level:

$$33\ \text{MeV/c}^2 \leqq M_{H^0} \leqq 210\ \text{MeV/c}^2.$$

The expected Higgs signal in the hadronic channel is shown in Fig. 7 together with the previous one. For completeness, the 99% confidence level limits on M_{H^0} were recalculated, combining all channels. To take properly into account the non-zero number of observed events and background expectation in the hadronic channel, the confidence level at a given Higgs boson mass is computed by treating the different channels separately. Each channel is thus described by a confidence level as defined in [16], using the expected signal, expected background and observed number of events in the considered channel. The confidence levels of all channels are then combined. The Higgs mass range excluded

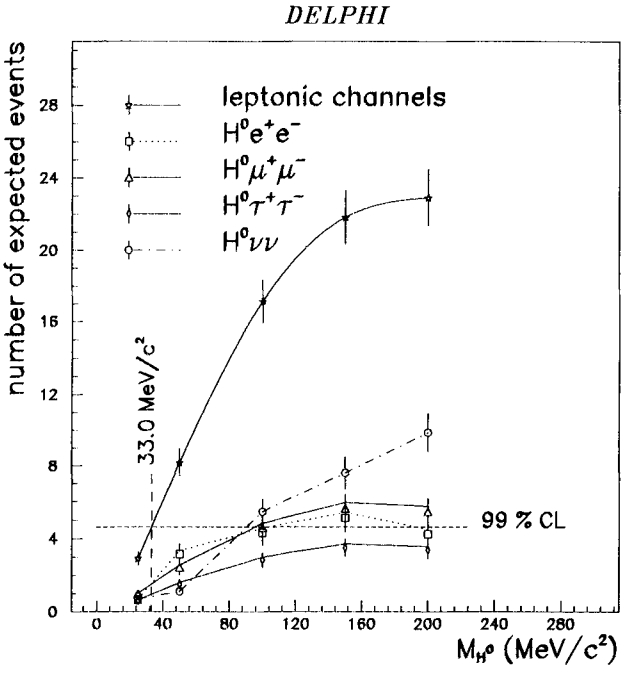

Fig. 6. Expected Higgs signal for leptonic channels only. The statistical and systematic uncertainties are added in quadrature. The 99% confidence level limit (straight line) corresponds to 4.6 events, which excludes the mass range from 33 MeV/c^2 to 210 MeV/c^2

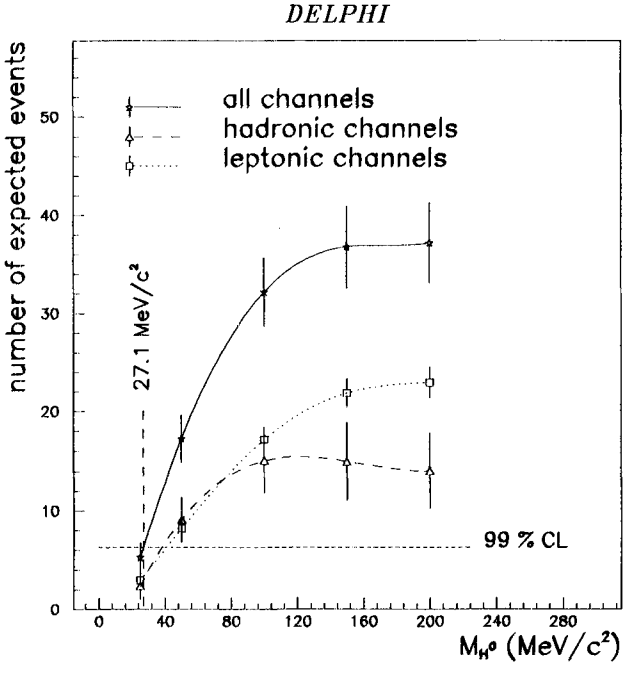

Fig. 7. Expected Higgs signal for leptonic and hadronic channels together. The statistical and systematic uncertainties are added in quadrature. The 99% confidence level limit (straight line) corresponds to 6.3 events, which excludes the mass range from 27 MeV/c^2 to 210 MeV/c^2. When decreasing the background expectation by one standard deviation, the 99% confidence level limit becomes 7.0 events which leads to a 2 MeV/c^2 increase of the lower bound of the excluded mass range

at the 99% confidence level then becomes:

$27\ \text{MeV/c}^2 \leqq M_{H^0} \leqq 210\ \text{MeV/c}^2$.

Decreasing the expected background by one standard deviation increases the lower bound of the excluded mass range by 2 MeV/c^2.

5 Conclusions for a standard model Higgs boson

Figure 8 shows the signal expected from a standard Higgs particle, when the analyses in Sects. 3 and 4 are combined, using only the leptonic channels. The full range below the muon threshold is excluded at more than 99% confidence level.

The error bars indicated in the figure contain both statistical and systematic uncertainties added in quadrature. The latter account mainly for the uncertainties on the Higgs selection efficiencies. Monte Carlo and data were compared in the distributions of the most crucial variables used in the selection procedure, showing that the systematic uncertainty on the Higgs selection efficiencies is about 5% for the analysis in Sect. 3 (see Tables 1 and 2), while it amounts to 10% for the second analysis (see Tables 3 to 7). The other large contribution comes from the uncertainty on the ratio of the Higgs boson to the hadronic Z^0 production cross sections, which is used to normalize the Monte Carlo results to the data when computing the expected signal. Both cross sections were calculated at lowest order, using the value 1/128 for α and the DELPHI measurements [17] for M_Z, Γ_Z and $\sin^2\theta_W$. It was checked that the Higgs production

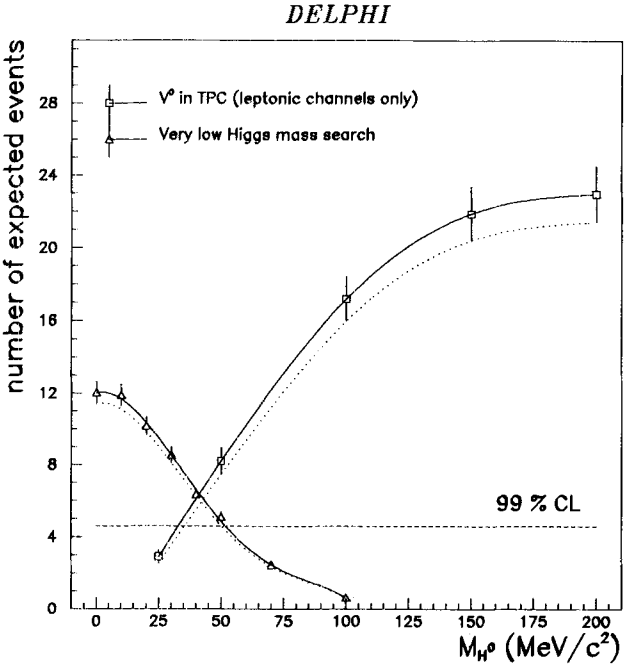

Fig. 8. Expected Higgs signal from the combined lepton channel analyses. The entire mass range below 210 MeV/c^2 is excluded at more than 99% confidence level for a standard model Higgs boson. Decreasing the expected signal by one standard deviation leads to the dashed curves

cross section is well behaved down to $M_{H^0}=0$. A 5% relative uncertainty on the cross section ratio was then introduced to account for the missing higher order corrections.

Figure 8 also shows the curves obtained when the expected signal is decreased by one standard deviation, which leaves the preceding conclusion unchanged.

6 Higgs boson in the MSSM

The results of the present search can be translated in terms of the minimal susy extension of the standard model (MSSM) described in [18]. All physical quantities, lifetimes, masses and cross sections, depend on two parameters. For this analysis, we choose the mass of the lightest scalar Higgs m_h and $\tan\beta = v_2/v_1$, where v_1 and v_2 are the vacuum expectations associated to the two Higgs doublets needed in MSSM.

To a good approximation, the $Z^0{*}h$ cross section is simply multiplied by a factor $\sin^2 2\beta$ with respect to the standard model predictions. The width $\Gamma(h \to e^+e^-)$ is multiplied by $\tan^2\beta$. One should also take into account the decay $h \to \gamma\gamma$ which can give large contributions when $\tan\beta$ is lower than 1. The calculation of this term suffers from well-known uncertainties coming from light quark masses. To be conservative, we use $m_u = m_d = 40\ \mathrm{MeV/c^2}$ as suggested in [18], which maximizes the two photon decay mode and reduces accordingly the efficiency of the two analyses. Figure 9 shows the domain excluded by the present search.

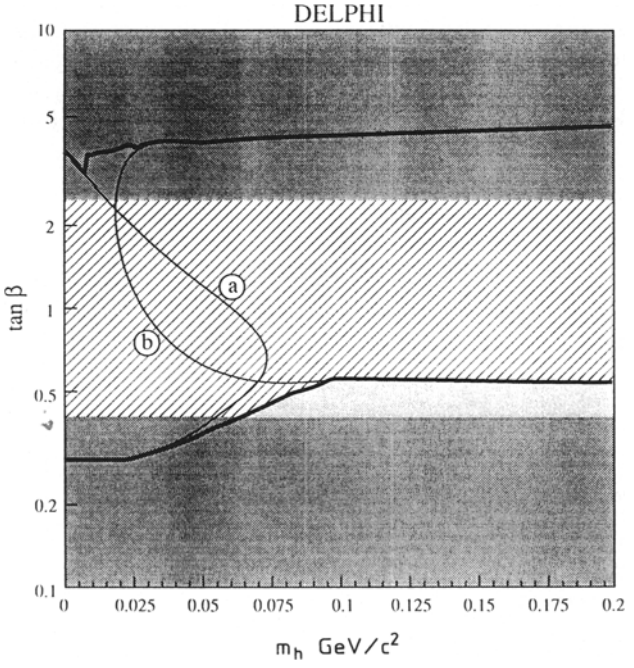

Fig. 9. MSSM limits given in terms of m_h, the mass of the light scalar boson and $\tan\beta$. The thick line indicates the domain excluded by combining the two searches based on $Z^0{*}h$ at the 95% confidence level. The thin line (*a*) gives the domain excluded by our search for a Higgs boson decaying outside the detector, while line (*b*) corresponds to the V^0 search using only leptonic decays of the Z^0. The two dark grey domains are excluded at the 95% confidence level by the invisible width measurement. The light grey domain at $\tan\beta \sim 0.5$ is also excluded at the 95% confidence level by combining the $hZ^0{*}$ and the invisible width limits. The hatched area indicates the domain excluded only by the $hZ^0{*}$ search with no overlap with the invisible width domain

For small values of $\sin^2 2\beta$, neutral Higgs bosons may be pair-produced through the decay $Z^0 \to hA$, where A, the CP odd neutral Higgs boson, is approximately degenerate in mass with h. The corresponding partial width is then given by $\Gamma(Z^0 \to hA) \sim 0.5\,\Gamma(Z^0 \to \nu\bar{\nu})\cos^2 2\beta$. In the region of interest, h and A will either decay into two charged particles, two photons or remain invisible. We checked that none of these final states populate significantly the final states of the standard channels. For instance, if h and A decay rapidly into e^+e^-, the final state may fulfill the selection criteria imposed on ordinary $Z^0 \to e^+e^-$ events since, in most cases, the two charged particles cannot be resolved in the TPC. These events are however easily recognized using the dE/dx measurements from the TPC wires which would give twice the energy deposit expected for relativistic particles. This analysis has been already performed in our search for heavy stable leptons [19] and shows that there are no such events.

We conclude that, in all cases, the hA final state does not correspond to any hadronic or leptonic channel selected for the determination of the partial widths in [17]. It will therefore appear as a residual width, which contributes to the so-called invisible width. Assuming the standard model value with three neutrino generations for the invisible width, one may deduce an upper limit for the hA contribution. Using $\Gamma_{\mathrm{inv}} = 469 \pm 29\ \mathrm{MeV/c^2}$, we find that $\Gamma(Z^0 \to hA) \leqq 39\ \mathrm{MeV/c^2}$ at the 95% confidence level. This result is translated into the limits shown in Fig. 9 which fully exclude the areas not covered by the $hZ^0{*}$ analysis.

7 Conclusions

Combining the search for an invisible Higgs boson with the search for a Higgs boson decaying into a V^0 inside the detector, we can exclude the existence of the Standard Model Higgs boson in the mass range between 0 and 210 MeV/c² at the 99% confidence level.

To constrain the MSSM Higgs sector, we combined the above analysis with our measurement of the invisible Z^0 width. Using in addition our previous results on a search for heavy MSSM Higgs particles [20], we can, for the first time, exclude at the 95% confidence level the existence of the lightest neutral Higgs boson, h, with a mass between 0 and 28 GeV/c², irrespective of the value of $\tan\beta$.

Acknowledgements. We are greatly indebted to our technical staffs, collaborators and funding agencies for their support in building and commissioning the DELPHI detector, and also to the many members of the LEP Division for the excellent performance of the LEP machine.

References

1. S.L. Glashow: Nucl. Phys. 22 (1961) 579; S. Weinberg: Phys. Rev. Lett. 19 (1967) 1264; A. Salam: Proceedings nobel symposium, ed. N. Svartholm, p. 367. Stockholm: Almqvist and Wiksells 1968
2. P.W. Higgs: Phys. Lett. 12 (1964) 132; Phys. Rev. Lett. 13 (1964) 508; Phys. Rev. 145 (1966) 1156; F. Englert, R. Brout: Phys. Rev. Lett. 13 (1964) 321
3. S.J. Freedman, J. Camp, M. Kroupa: Phys. Rev. Lett. 52 (1984) 240; M.J. Savage, B.W. Filippone, L.W. Mitchell: Phys. Rev. Lett. D37 (1988) 1134; D. Kohler, B.A. Watson, J.A. Becker: Phys. Rev. Lett. 33 (1974) 1628; I. Beltrami et al.: Nucl. Phys. A451 (1985) 679; R. Barbieri, T.E.O. Ericson: Phys. Lett. 57B (1975) 270
4. M. Davier, H. Nguyen Ngoc: Phys. Lett. B22 (1989) 533
5. ALEPH Coll., D. Decamp et al.: Phys. Lett. B236 (1990) 233; ALEPH Coll., D. Decamp et al.: Phys. Lett. B245 (1990) 289
6. OPAL Coll., M.Z. Akrawy et al.: Phys. Lett. 251B (1990) 211
7. L3 Coll., B. Adeva et al.: Phys. Lett. 252B (1990) 518
8. DELPHI Coll., P. Aarnio et al.: CERN PPE/90-128 to be published in N.I.M.
9. DELPHI Coll., P. Abreu et al.: Phys. Lett. B241 (1990) 435
10. F.A. Berends, R. Kleiss: Nucl. Phys. B260 (1985) 32
11. R. Kleiss et al., in: Z physics at LEP 1, CERN Report-89-08, eds G. Altarelli, R. Kleiss, C. Verzegnassi, Vol. III, p. 69. Geneva: CERN 1989
12. J.E. Campagne, R. Zitoun: Z. Phys. C – Particles and Fields 43 (1989) 469
13. P.J. Franzini et al., in: Z physics at LEP 1, CERN Report-89-08, eds G. Altarelli, R. Kleiss, C. Verzegnassi, Vol. II, p. 59. Geneva: CERN 1989
14. E.W.N. Glover et al., in: Z physics at LEP 1, CERN Report-89-08, eds G. Altarelli, R. Kleiss, C. Verzegnassi, Vol. II, p. 11. Geneva: CERN 1989
15. DELPHI Coll., P. Aarnio et al.: Phys. Lett. B241 (1990) 425
16. Particle Data Group, Review of particle properties, Phys. Lett. B239 (1990), section III-28
17. DELPHI Coll., P. Abreu et al.: CERN-PPE/90-119 (unpublished)
18. S. Dawson, J.F. Gunion, H.E. Haber, G.L. Kane: Higgs hunter's guide, Menlo Park: Addison Wesley 1989, and references therein
19. DELPHI Coll., P. Abreu et al.: CERN-PPE/90-167 (unpublished)
20. DELPHI Coll., P. Abreu et al.: CERN-PPE/90-163 (unpublished)